End-Effects in Diblock Copolymer Melts

A THESIS
SUBMITTED TO THE FACULTY OF THE GRADUATE SCHOOL
OF THE UNIVERSITY OF MINNESOTA
SCHOOL OF PHYSICS AND ASTRONOMY
BY

Mark Mackey

IN PARTIAL FULFILLMENT OF THE REQUIREMENTS
FOR THE DEGREE OF
MASTER OF SCIENCE

Advisor:
David C. Morse

January 2018

Acknowledgements

I would like to thank Professor David Morse for being a fantastic advisor. Without his patient guidance and his incredible depth of knowledge I would not have been able to complete this project. I am very grateful to have had the opportunity to work with him.

I am indebted to the graduate students in Professor Morse's research group with whom I've had the pleasure of sharing an office over the course of this project. In addition to running the metadynamics simulations, Taher Ghasimakbari has been a wonderful friend and has helped answer countless questions I asked asked him. Josh Mysona also answered numerous questions of mine. Mridul Yadav ran one-dimensional SCFT simulations for comparison to one of the measurements presented in this thesis and also answered many of my questions.

I would also like to thank the Minnesota Supercomputing Institute for providing the computational resources with which we obtained all of the simulation results presented here.

Dedicated to my grandfather, Thomas W. Nelson

Abstract

Modern understanding of block copolymer systems relies heavily on coarse-grained models and mean-field theories such as self-consistent field theory (SCFT) and Fredrickson-Helfand (FH) theory. These models simplify the system, ignoring the finer structural details of the underlying polymers. One often ignored detail is the difference in the chemistry of the last monomer on the chain. Polymer synthesis requires the end-monomer to have a different chemistry than the other monomers in the chain. The effect that this difference has on equilibrium properties of the system has not been thoroughly explored. This work is an attempt to quantify these effects using course-grained simulations.

We report on a number of simulation measurements designed to characterize the local environment of the end-monomer. The local composition distributions of monomers around the end-monomer was measured and compared to the other monomers. Additionally the composition profile of all monomer types was measured and compared to 1-dimensional SCFT simulations.

Our second focus was to quantify the shift in position of the Order-Disorder Transition (ODT) due to an end-monomer that was more repulsive than the other beads in the chain. Upper and lower bounds on the new position of the ODT were calculated using conventional scattering structure factor hysteresis loop methods. A subsequent Claperyon-style approximation of the new position of the ODT agreed nicely with the range that was measured. The precise location of the ODT was then obtained using well-tempered metadynamics simulations. Finally, we estimated the effective interaction parameter χ_e by fitting disordered phase scattering measurements to Renormalized One Loop (ROL) theory predictions. This was used to determine the effect that the repulsive end-monomer had on the value $\chi_e N$ at the ODT. Our results indicate that the effect is small enough to go unnoticed when the calibration of χ_e is constrained to scattering data from a single chain-length.

Table of Contents

List of Tables

List of Figures

Chapter 1

Introduction

1.1 Background

Polymers are large chain molecules composed of repeating chemical units called monomers. The simplest polymers are linear chains constructed from a single type of monomer and are called homopolymers. Copolymers are polymers containing two different monomers. This thesis is concerned with a particular class of linear copolymers called diblock copolymers, where the two monomer types are grouped together into 2 blocks (for example, ...-A-A-A-B-B-B-...). Here we use coarse-grained simulation models to study dense, nearly incompressible melts of diblock copolymers in which unlike monomers interact with a repulsion stronger than that of monomers of the same type. If the two blocks of each chain were not covalently bonded together, the resulting homopolymers would macroscopically phase separate. Instead, the blocks will group together and form regions rich in A and B monomers to minimize contact between dissimilar monomers. The degree to which the two monomer species segregate depends on the magnitude of the free energy penalty for mixing. In a mixture with a positive enthalpy of mixing, the tendency to demix increases with decreasing temperature. In this case, if the temperature is above a critical value T_{ODT}, entropy dominates, and the system will remain in a spatially homogeneous mixed (disordered)

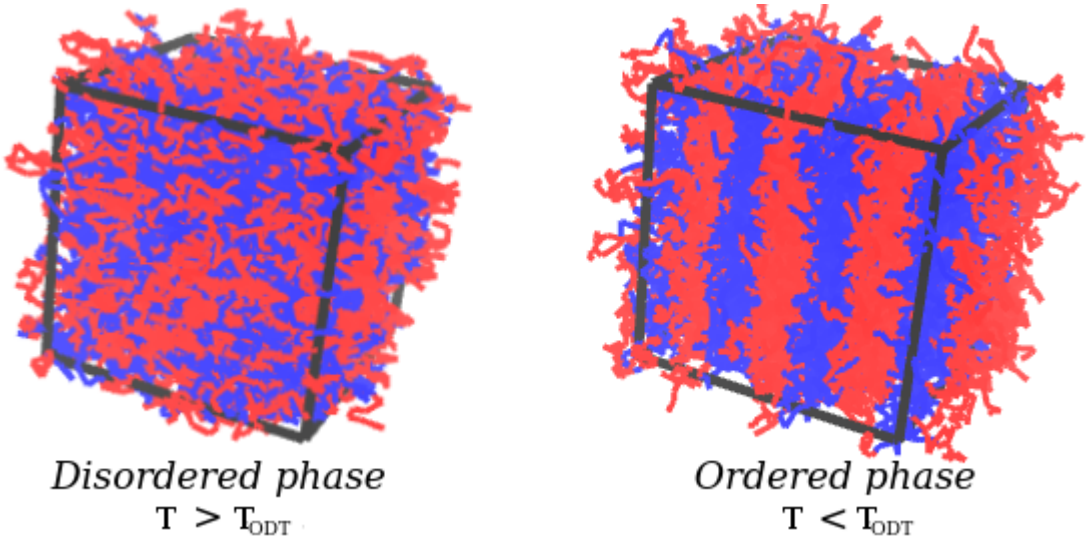

Figure 1.1: Disordered and ordered phases of symmetric diblock copolymer melts.

state. If the temperature falls below T_{ODT}, the system will undergo a weak first-order phase transition and form a spatially periodic ordered structure. The geometry of the resulting ordered structure depends on the ratio of A and B monomers in each chain. In the case of symmetric diblock copolymers, in which the two blocks contain equal number of monomers, the system forms the lamellar (layered) structure Figure 1.1.

1.2 Theoretical Models

Initial attempts to understand polymer mixtures relied on Flory-Huggins [1] [2] theory. We discuss Flory-Huggins theory here only for the purpose of providing context and comparison to later theoretical models of polymer liquids. Flory-Huggins theory is a lattice model that describes the thermodynamics of homogeneous polymer mixtures. In its most general form, the free energy of mixing per monomer Δf is expressed as

a sum of the form

$$\Delta f = kT \sum_i \frac{\phi_i}{N_i} \ln \phi_i + \Delta f_{\text{int}}(\phi, T) \tag{1.1}$$

where N_i is the degree of polymerization of species i, for $i = A$ or B, $\phi_A = \phi$ and $\phi_B = 1 - \phi_A$ are volume fractions, kT is thermal energy, and $\Delta f_{\text{int}}(\phi, T)$ is an interaction free energy per monomer. The first term in this expression is the entropy of mixing an ideal gas which can conceptualized as the entropy associated with placing the ends of the chains on the lattice. The other monomers don't enter into the calculation because it is assumed that the conformational entropy of a single chain is the same when it is alone on a lattice or mixed with other chains. It is important to stress that the internal energy per monomer $\Delta f_{\text{int}}(\phi, T)$ is assumed to be independent of chain length and is sensitive only to the local structure of the polymer liquid (nearest-neighbor interactions). This is combined with a random mixing approximation in which it is assumed that the local structure of the liquid around any given monomer is the same as the average structure of the liquid as a whole. This yields an expression for Δf_{int} of the form:

$$\frac{\Delta f_{\text{int}}}{k_B T} = \chi \phi_A \phi_B \tag{1.2}$$

where the dimensionless proportionality constant χ is known as the Flory-Huggins interaction parameter.

The primary theoretical model used to study polymer mixtures has been polymer self-consistent field theory (SCFT) [3]. SCFT is a coarse-grained density functional theory in which polymers are treated as continuous random walks. SCFT yields a free energy functional $G[\langle c \rangle]$ as a functional of the average monomer concentration that can be expressed as a sum

$$G[\langle c \rangle] = G_{\text{chain}}[\langle c \rangle] + G_{\text{int}}[\langle c \rangle] \tag{1.3}$$

where $G_{\text{chain}}[\langle c \rangle]$ is the free energy of an ideal system of non-interacting chains $G_{\text{int}}[\langle c \rangle]$ is the contribution from interactions between chains. The symbol $\langle c \rangle$ is used here to represents a two component field $\langle c(\mathbf{r}) \rangle = (\langle c_A(\mathbf{r}) \rangle, \langle c_B(\mathbf{r}) \rangle)$ with components $\langle c_A(\mathbf{r}) \rangle$ and $\langle c_B(\mathbf{r}) \rangle$ that denote the average concentration of A and B monomers at position $\mathbf{r}$. The most common form of the theory assumes that the polymer liquid is incompressible, so that $\langle c_A(\mathbf{r}) \rangle + \langle c_B(\mathbf{r}) \rangle$ is equal to a constant total monomer concentration c. In this limit, the free energy can also be expressed as a functional of the volume fraction $\phi_A(\mathbf{r})$ of A monomers at each position, defined such that $c_A(\mathbf{r}) = c\phi_A(\mathbf{r})$. The simplest and most common form of SCFT assumes that the contribution to the free energy due to interactions between polymer chains $G_{\text{int}}[\langle c \rangle]$ is given by an expression

$$\frac{G_{\text{int}}}{k_B T} = \chi_e c \int \phi_A(\mathbf{r}) \phi_B(\mathbf{r}) d\mathbf{r} \tag{1.4}$$

defined similarly to (1.3), in which χ_e is an effective Flory-Huggins interaction parameter.

In this thesis, we consider a melt of diblock copolymers containing M chains in a total volume V. Each chain has a degree of polymerization N, giving a total monomer concentration $c = MN/V$. Polymer chains are treated as random walks with statistical segment lengths b_A and b_B for A and B monomers, respectively. Let f_A denote the volume fraction of A monomers in each chain, with $f_A = 1/2$ in the symmetric case that we focus on here. Let $R_{e0} = N^{1/2} b$ denote the random-walk end-to-end length of each chain in a uniform state. The thermodynamic state of an incompressible polymer liquid is specified in SCFT by the dimensionless parameters $\chi_e N$, f_A, and the ratio b_A/b_B.

Because SCFT is a mean-field theory, predictions are only valid in regions where composition fluctuations are relatively small. For this reason, SCFT is least accurate

near the order-disorder transition (ODT) where fluctuations become large. Leibler [4] showed that, for symmetric diblock copolymer melts, SCFT predicts a transition between the disordered and lamellar phases at a critical value of $\chi_e N = 10.495$. SCFT predicts that, in this case, the transition should be second-order transition in which a periodic modulation of the composition appears for $\chi_e N > 10.495$, but in which the magnitude of this modulation approaches zero at the critical value of $\chi_e N$. Leibler also pointed out, however, that earlier work by Brazovskii on weak first-order crystallization transitions [5]) implied that this phase transition must actually become first order as a result of the appearance of strong composition fluctuations near the ODT.

The Fredrickson-Helfand (FH) theory [6] incorporated fluctuation effects into SCFT by adapting Brazovskii's theory of weak crystallization to describe the ODT of symmetric and nearly symmetric diblock copolymers. In this theory, the magnitudes of predicted corrections to SCFT predictions for various quantities are controlled by the dimensionless parameter

$$\overline{N} = N(b^3 c)^2 \quad , \tag{1.5}$$

sometimes referred to as the invariant degree of polymerization. We recall that the root-mean-squared end-to-end length of a random walk is $R_{e0} = N^{1/2} b$, and that the volume pervaded by a chain is approximately $V \approx R_{e0}^3$. The volume actually occupied by the chain is $v_{\text{mon}} N = N/c$. Note that $\overline{N}^{1/2} = \sqrt{N} b^3 / c$ is equal to the ratio $R_{e0}^3 c/N$ of pervaded to occupied volumes. This parameter is thus measure of the degree of overlap among chains in a dense polymer liquid. The FH theory predicted that the magnitude of corrections to SCFT predictions should decrease with increase $\overline{N}$, thus recovering SCFT predictions in the limit of $\overline{N} \to \infty$. The incorporation of fluctuation effects into SCFT increases the predicted location of the ODT in symmetric diblock copolymers to $\chi_e N = 10.5 + 41.0 \overline{N}^{-1/3}$.

The FH theory and its immediate descendants [7] [8] [9] [10] [11] were designed to describe only the dominant effects of strong composition fluctuations very near the ODT for long chains. Several authors attempted to construct more complete theories of corrections to SCFT, but reported technical difficulties. The most serious conceptual problem arose from the fact that predictions were found to be sensitive to the treatment of short wavelength correlations, at length scales of order the monomer size that the underlying models were never designed to describe. A more recent "renormalized one loop" (ROL) theory developed by Grzywacz, Qin, and Morse [12] showed that this ambiguity could be removed by adapting a standard technique used in quantum field theory known as renormalization, in which the contributions arising from very short-wavelength fluctuations are absorbed into a redefinition or "renormalization" of several parameters in the model. When applied to this problem, procedure allowed short-wavelength (i.e., ultraviolet) divergences in analytic predictions for measurable quantities to be absorbed into a redefinition of the statistical segment length and the effective interaction parameter χ_e. The ROL theory has since been shown to provide accurate description of collective and intramolecular correlations in the disordered phase of a symmetric block copolymer melt, as discussed below.

1.3 Analysis of Simulations

When attempting to compare results between any combination of theory, simulation, and experiment, one of the biggest challenges is estimating the value of the effective interaction parameter χ_e for a given simulation model or chemical system. Coarse-grained theories such as SCFT and the ROL theory require a value for χ_e as an input parameter. Experimental or simulation data must be fit to some theoretical prediction to estimate how χ_e depends on temperature in experiment or on some

other control parameter in simulations.

Morse and coworkers [13] recently made significant advances in the interpretation of coarse-grained simulations of symmetric diblock copolymers, which have allowed consistent results to be obtained from a variety of different simulation models. Their success in this relied critically on the development of an adequate method of estimating the relationship between χ_e and the parameters that one varies in a simulation. The method that they developed had two elements. The first was use of an appropriate form of thermodynamic perturbation theory to construct an approximation for χ_e that is accurate in the limit of small values of χ_e, and that did not involve any fitting to determine adjustable parameters. The second was the use of a fit of results for the structure factor $S(q)$ in the disordered phase to predictions of the ROL theory. Analysis of the disordered phase showed that the ROL theory could provide an excellent simultaneous fit to results for $S(q)$ from several different simulation models over a wide range of chain lengths and values of $\chi_e N$ (universality). A subsequent investigation of the ODT [14] showed that simulation measurements of a variety of thermodynamic quantities including the free energy per chain, the value of $(\chi_e N)_{\mathrm{ODT}}$, the latent heat of transition, and the layer spacing agreed across all models when the resulting calibration of χ_e was used to plot data and to compare results obtained from different models. Specifically, the value of $(\chi_e N)_{\mathrm{ODT}}$ for all the simulation models studied was shown to collapse onto a common curve when plotted vs. $\overline{N}$. The resulting relationship for $(\chi_e N)_{\mathrm{ODT}}$ as a function of $\overline{N}$ was well approximated by a function

$$(\chi_e N)_{\mathrm{ODT}} = 10.495 + 41.0\bar{N}^{-1/3} + 123.0\bar{N}^{-0.56}. \tag{1.6}$$

Equation (1.6) reduces to the SCFT prediction in the limit $\bar{N} \to \infty$. The first two terms are the same as Fredrickson-Helfand theory, while the last was added empirically

to fit the data. The models presented in these studies span $\bar{N} \approx 100-7600$, overlapping the experimental range of $\bar{N} \approx 200 - 20000$.

1.4 Analysis of Experiments

Gillard et al. [15] have recently presented an unusually precise analysis of experimental results for a model diblock melt to the body of simulation data in Ref. [13]. Results of small-angle neutron and X-ray scattering measurements conducted on one poly(1,4-isoprene-b-DL-lactide) diblock copolymer melt in the disordered phase were fit to ROL theory predictions in order to estimate the temperature dependence of $\chi_e(T)$. The resulting calibration of $\chi_e(T)$ was then used to compare simulation and experimental results for the peak wavenumber q^* at which the structure factor is maximum, and the value of $\chi_e N$ at the ODT, and the latent heat of transition, which had been measured for this sample using unusually sensitive calorimetry experiments.

To study the behavior of the peak wavenumber, Gillard et al. plotted experimental results for q^* as a function of the dimensionless quantity $\chi_a^* N \equiv 10.495 - cNS^{-1}(q^*)/2$ alongside ROL predictions for this relationship. Plotting this way allowed them to compare experimental results for q^* to ROL predictions without having to estimate how $\chi_e(T)$ depends on T. Measured values of q^* were found to be smaller than ROL predictions by approximately 10%. It was initially assumed that this discrepancy was due to deviations from the literature values of the statistical segment lengths b_A and b_B. To correct this, b_A and b_B were scaled by approximately 20% until the ROL theory agreed with scattering measurements. The authors noted that a correction of this magnitude was difficult to justify, but in the absence of a fundamental reason to reject this analysis, they continued to use the scaled statistical segment lengths in their analysis of other properties.

Gillard et al. also compared experimental and simulation results for the value $(\chi_e N)_{\text{ODT}}$ of $\chi_e N$ at the transition. This involved simply evaluating $\chi_e(T)$ at the observed transition temperature, using the calibration of $\chi_e(T)$ that was obtained by analyzing small-angle scattering from the disordered phase of one of several samples with different molecular weights. The resulting estimate for $(\chi_e N)_{\text{ODT}}$ for the sample that was used to estimate $\chi_e N$ exceeded the value obtained from simulations at the same value of $\overline{N}$ by an amount slightly greater than the known experimental uncertainty. When the same estimate of $\chi_e(T)$ was used to analyze data gathered from other samples composed of chains of somewhat greater molecule weights, however, the resulting estimates of $(\chi_e N)_{\text{ODT}}$ exceeded simulation results by significantly greater amount, which was well outside the expected experimental error bars.

The fact that the estimate of $\chi_e(T)$ used in this did not appear to be transferable between samples with different molecular weight led the authors to speculate that this discrepancy could be a result of an end-group contributions to the free energy of mixing in PI-PLA diblock copolymers. The chemical basis for this explanation was the observation that the poly(DL-lactide) (PLA)-terminal end-segment of the block polymer contained a hydroxyl (OH) group that could interact with the PLA backbone carbonyl groups through a hydrogen-bonding interaction. The resulting attraction of the end-monomer to other monomers on the same block would favor de-mixing and thus lead to an estimate of $\chi_e(T)$ that was somewhat larger than it would be in the absence of this effect. The importance of the end group contribution is expected to increases as N decreases, because the relative contribution to the total χ_e due to the end-group increases as chain length N decreases.

One other important way in which the experimental systems studied by Gillard et al. differed from the simulations to which they were initially compared is that the real polymers have a significant polydispersity in the degree of polymerization, whereas

the model used in the simulations were strictly monodisperse. Beardsley and Matsen subsequently published a further investigation [16] of the same set of experimental data [15] in a manner that explicitly took into account the effects of polydispersity. They did this by comparing experimental data to a polydisperse version of the simulation model from Ref. [13]. The relationship between χ_e and simulation parameters for this model was calibrated by matching measurements of $S(q)$ from corresponding monodisperse simulations in the disordered phase to ROL theory predictions, which thus far exist only for monodisperse systems. Simulations were then rerun with a polydisperse configuration of the model with a polydispersity index similar that of the experimental system that was used in small-angle scattering experiments, in order to determine the dependence of $S(q^*)$ on $\chi_e N$ for a system with appropriate polydispersity. The results of these polydisperse simulations could then be directly compared to experimental results in order estimate the temperature dependence of $\chi_e(T)$ in the experiments and to test the level of agreement for other quantities. Simulation results for q^* were found to match nearly exactly without further adjustment. This showed that the discrepancy between experimental results and ROL predictions or simulation results for q^* was primarily a result of polydispersity. Values for $(\chi_e N)_{\text{ODT}}$ from simulations and from experiments on the sample used in scattering experiments also agreed extremely well.

The analysis of the data of Gillard *et al* by Beardsley and Matsen focused, however, exclusively on analysis of the single sample that was used in extensive scattering experiments. Data from this sample was compared to results of a simulation of a single system designed to have matching average chain length and polydispersity. Their re-analysis did not discuss or analyze any of the measurements of the ODT obtained from the samples with somewhat longer chain lengths. The difference in the values $(\chi_e N)_{\text{ODT}}$ obtained by Gillard et al. for samples with molecular weights

that differ by about 50% was much larger than that relatively small difference seen over this range in simulations of monodisperse polymers, and opposite in sign to the difference expected on the basis of these simulations: Simulations and theory both predict a value of $(\chi_e N)_{\mathrm{ODT}}$ that decreases with increasing $\overline{N}$, but Gillard *et al.* obtained a higher value of $(\chi_e N)_{\mathrm{ODT}}$ for higher molecular weight samples. Gillard et al. suggested that this unexpected chain length dependence could be the result of an end-group effect. If so, however, this raises the question of how Beardsley and Matsen could have gotten such excellent agreement by comparing experiment on a system that may or may not have an significant end-group effect to a simulation model that clearly did not have a signficant end-monomer effect. The work presented in this thesis is motivated in part by this question.

1.5 Motivation and Outline

This work is specifically concerned with quantifying the effects of changing the chemistry of the last monomer in the chain, hereafter referred to as the end-monomer. The standard theoretical models previously discussed assume that each monomer of the same type is chemically identical as a matter of convenience. This assumption is particularly inaccurate when applied to the end-monomer; the lack of a second covalently bonded neighbor requires it to either be highly reactive or have an additional chemical group bonded to it. This group can cause the end-monomer to interact differently with its neighbors than the other monomers on the chain (hereafter this will be referred to as the end-monomer effect). The purpose of this work is to understand how the end-monomer effect shifts the location of the order-disorder transition and to characterize the local environment around end-monomer using molecular dynamics simulations. This analysis will also help us understand if end-monomer effects can

reasonably explain the chain length dependence of $(\chi_e N)_{\text{ODT}}$ reported by Gillard et al. in Ref. [15].

Previous simulation studies of symmetric diblock copolymers near the ODT [14] have suggested that the disordered and ordered phases near the ODT are both relatively strongly segregated structures with similar local degree of segregation. These simulations with values of $\overline{N}$ typical in many experiments give values for $(\chi_e N)_{\text{ODT}}$ that are approximately 2x the SCFT prediction. SCFT calculations of the structure of the ordered phase at the resulting value of $\chi_e N$ predict a structure with strongly segregated, nearly pure domains of A and B, and are in rather close agreement with results of simulations of ordered structures. Measurements of the A-B pair energy on each side of the ODT showed a change of only around 6% in the amount of AB contact. Measurements of the distribution of local compositions around each monomer were also extremely similar in both phases. All of these results as well as visualization of simulation results strongly suggested that both the disordered and ordered phases near the ODT are relatively strongly segregated structures with a degree of segregation similar to that predicted by SCFT for the ordered phase. It is known that for values of $\chi_e N$ much greater than mean field ODT, both blocks of a diblock copolymer became stretched away from the interface, pulling the end-monomers towards the center of the domain. This is illustrated in Figure 1.2. Given this picture of the ordered and disordered phases, one might expect that the end-monomer would be buried deep in a region rich in monomers of the same type as its own block. This would reduce the effect that any attraction to its own species (or equivalently repulsion from the other species) would have on thermodynamics. One goal of a simulation study of end-group effects it thus to quantify the probability of an end-group of a B block of an AB diblock copolymer coming into contact with an A monomer in either the ordered or disordered phase, and to determine how this is related to the shift in

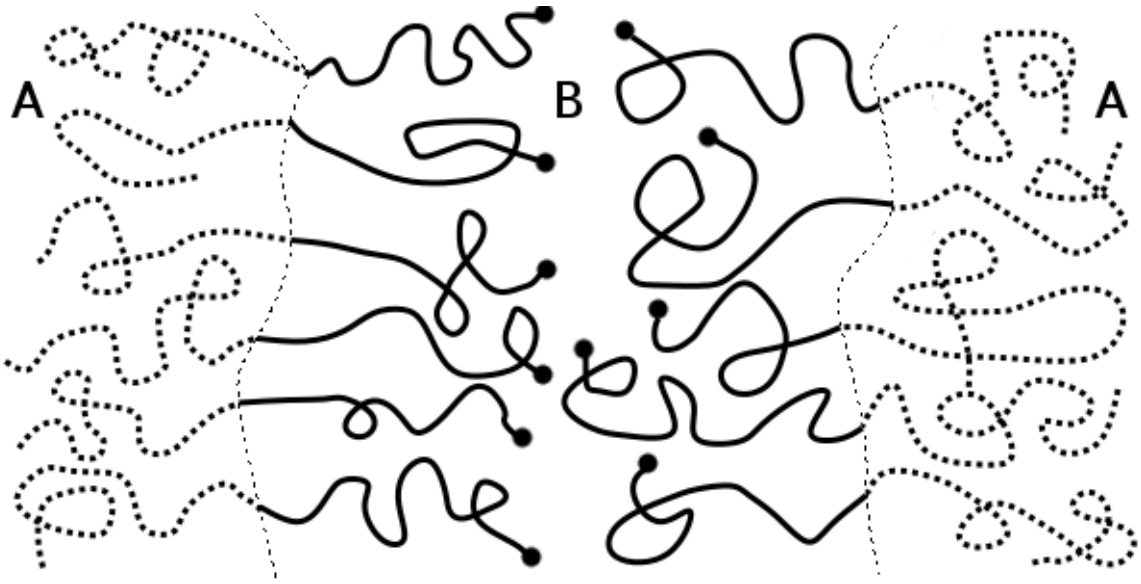

Figure 1.2: Local segregated regions near the ODT in the disordered phases. The end-monomer on the B-block is illustrated by a dot.

the ODT caused by a chemically distinct end group.

This thesis is organized as follows. The rest of Chapter 1 gives an overview of the simulation models studied throughout this work. Chapter 2 details various simulation measurements used to contrast the local environment of the end-monomer with that of the other monomers. Chapter 3 details the different techniques used to determine the new position of the ODT resulting from the end-monomer effect. These techniques include a structure factor hysteresis loop, a Clayperon-style coexistence curve approximation, and well-tempered metadynamics simulations. The final section of Chapter 3 addresses the impact that the end-monomer effect has on $(\chi_e N)_{\mathrm{ODT}}$. This is done by fitting scattering measurements in the disordered phase to ROL theory predictions to estimate the value of χ_e as a function of our control parameter.

Chapter 2

Simulation Methods

2.1 Simulation Model

The simulation reported in this thesis are molecular dynamics (MD) simulations of a simple bead-spring model with soft pair interactions similar to those originally introduced by Groot and coworkers [17] for use in dissipative particle dynamics. The particular model studied here is a variant of one studied in previous work by coworkers in my research group [13], in which it was referred to as model S1.

In the model studied here, bonded pairs of beads interact via a harmonic bond potential of the form [18]

$$V_{\text{bond}}(r) = \frac{\kappa}{2} r^2. \tag{2.1}$$

The non-bonded pair interaction potential between two monomers i and j is of the form

$$V_{ij} = \epsilon_{ij} u(r) \tag{2.2}$$

where ϵ_{ij} is a prefactor and $u(r)$ is a unitless function

$$u(r) = \begin{cases} \frac{1}{2}\left(1 - \frac{r}{\sigma}\right)^2 & r \leq \sigma \\ 0 & r > \sigma \end{cases}. \tag{2.3}$$

For diblock copolymer systems involving monomer types A and B we use $\epsilon_{AA} = \epsilon_{BB} = \epsilon$ and the repulsion strength between A and B monomers is characterized by a parameter

$$\alpha \equiv \epsilon_{AB} - \epsilon_{AA}. \tag{2.4}$$

Thus the pair energy matrix ϵ_{ij} can be written as

$$\epsilon_{ij} = \begin{bmatrix} \epsilon & \epsilon + \alpha \\ \epsilon + \alpha & \epsilon \end{bmatrix} \tag{2.5}$$

In these simulations, α is manipulated as a control parameter to vary the free energy cost of contact between A and B monomers.

All simulations are isothermal, isobaric MD simulations carried out at a constant temperature T and constant pressure P. Temperature and pressure are controlled using a Nose-Hoover thermostat and Martyna-Tucker-Klein barostat. The target value for the pressure P was previously chosen[14] so as to give a monomer concentration $c = 3.0$ in the limit $\alpha = 0$, $N \to \infty$. Most simulations were carried out using the "simpatico" C++/MPI simulation package, which was developed in the Morse research group.

Numerical values for the simulation parameters that are common to all simulations presented here are given in Table 2.1.

Simulation Parameter		Value
Base Interaction Energy	ϵ	25.0
Interaction Radius	σ	1.0
Bond Spring Constant	κ	3.406
Monomer Concentration	c	3.0
Temperature	kT	1.0
Pressure	P	20.249

Table 2.1: Model simulation parameters

2.2 Modeling the End-Monomer Effect

In order to model the end-monomer effect, we simulate a modified model of a symmetric AB diblock copolymer in which the last monomer on the B block is treated as a monomer of a distinct type, which we will call type C. This is equivalent to simulating a linear ABC triblock copolymer of N monomers in which the terminal C block contains only one monomer, the A block contains $N/2$ monomers, and the B block contains $N/2-1$ monomers. To generalize our model of interactions, we take a common value of

$$\epsilon_{AA} = \epsilon_{BB} = \epsilon_{CC} = \epsilon \tag{2.6}$$

for the prefactors of interactions between similar monomers, and define a parameter

$$\alpha_{ij} = \epsilon_{ij} - \epsilon \tag{2.7}$$

to characterize the how much the interactions between dissimilar monomers differ from ϵ. In all of the simulations presented here we set $\alpha_{BC} = 0$, or $\epsilon_{BC} = \epsilon$, so that the interaction between B monomers and the end monomer in the same block are the same as interactions between similar monomers. An additional repulsion between the last monomer of the B block is introduced (if at all) by using a value of $\alpha_{AC} \geq \alpha_{AB} \geq 0$.

In Chapter 2, we are interested in characterizing the environment around the end-monomer while leaving it chemically identical to the other B monomers. In chapter 2, we thus constrain

$$\alpha_{AC} = \alpha_{AB} \quad , \tag{2.8}$$

or $\epsilon_{AC} = \alpha_{AB}$.

In Chapter 3, we consider the how the introduction of a chemically distinct end-monomers effects the order-disorder transition, by using a model with $\alpha_{AC} > \alpha_{AB}$. In

order to minimize the number of independent parameters in the model, however, we somewhat arbitrarily add the constraint that

$$\alpha_{AC} = 1.4\alpha_{AB} \quad . \tag{2.9}$$

With this choice, the pair energy matrix becomes (2.5) becomes

$$\epsilon_{ij} = \begin{bmatrix} \epsilon & \epsilon + \alpha & \epsilon + 1.4\alpha \\ \epsilon + \alpha & \epsilon & \epsilon \\ \epsilon + 1.4\alpha & \epsilon & \epsilon \end{bmatrix} \tag{2.10}$$

where $\alpha \equiv \alpha_{AB}$. We show in chapter 3 that this choice yields a small but easily measurable shift in the value of α at the ODT.

In order to take full advantage of previous simulations of diblock copolymers using the same model, we have created triblock configurations that closely match those used in previously studied diblock copolymer configurations [14]. In an NPT simulation in a cubic simulation cell, the average system is controlled by choosing the total number of molecules in the system, denoted here by M. The value of M used in these configurations was chosen in previous work so that the layer spacing in an ordered phase with three layers oriented along one of the primary axes of a cubic simulation cell has a layer spacing equal to the equilibrium spacing at the ODT of the diblock copolymer. This is intended to yield a system in which the box remains nearly commensurate near the ODT of a system with a modest end-monomer effect.

N	Simulation Parameter		Diblock	Triblock
16	Number of Chains	M	2007	2007
	Chain Length	N	16	16
	Box Length	L	22.038	22.038
	Chain Composition		8A+8B	8A+7B+1C
32	Number of Chains	M	2555	2555
	Chain Length	N	32	32
	Box Length	L	30.094	30.094
	Chain Composition		16A+16B	16A+15B+1C

Table 2.2: System configurations for diblock and triblock configurations

Chapter 3

Environment of the End-Monomer

How much the existence of a distinct end-monomer at one end of a diblock copolymer effects the behavior of the system depends, among other things, on the extent of contact between the end monomer and monomers of the other two monomer types. In this chapter, we present two measurements that characterize the local environment of a C end monomer at the end of the B block of an AB block copolymer, and examine how much the environment of a C monomer differs from that of a randomly chosen B monomer. The results presented in this chapter were all obtained from simulations in which pair interactions involving the C end monomer are taken to be the same as those used for a B monomer, by taking $\epsilon_{CC} = \epsilon_{BC} = \epsilon_{BB}$ and $\epsilon_{AC} = \epsilon_{AB}$. The potential energy used in these simulations thus does not distinguish B and C monomers. For bookkeeping purposes, however, we treat the end monomer as being a monomer of a distinct type. These measurements thus explore the extent to which the environment of the end monomer in both the disordered and ordered phase differs from that of other monomers in the B block purely as a result of the chemical location of the C monomer at the end of the chain, rather than as a result of differences between AB and AC interactions.

3.1 Distributions of Local Compositions

It this section, we quantify the extent to which the composition of the local environment around an end-monomer at the end of the B block of an AB diblock copolymer is different than that of a randomly chosen B monomer. Deep within the disordered phase we would expect little or no difference in the composition (i.e., the relative number of A and B monomers) of the monomers surrounding a B or C monomer. As χ_e is increased, however, and the system develops well-defined A- and B- domains, we might expect the end monomer to have somewhat less contact with A monomers than other monomers in the B block, because the end-monomer is furthest from the A/B junction, and because we might expect the B block to be somewhat stretched away from the A/B interface. If so, the lower level of contact between A and C monomers would tend to decrease how strongly a stronger repulsion between A and C monomers would effect the structure and thermodynamics of such a system. The results presented here show, however, that the differences between the environment of B and C monomers is in fact quite small in both the disordered and ordered phase near the order-disorder transition.

To quantify the composition of the environment of a monomer, we define a local mole fraction ϕ_A and $\phi_B = 1 - \phi_A$ of neighboring monomers around every monomer in a system. To define these quantities, we define a sum S_A and S_B for each monomer in the system, in which S_i is the sum of weights of intermolecular neighbors of type i near a test monomer, in which each monomer of type i within a distance 1.5σ of the test monomer is assigned a weight given by a smeared step-function

$$f(r) = \left(1 + e^{12(r-r_c)/r_c}\right)^{-1} \quad . \tag{3.1}$$

In this calculation, a type-C neighbor (the end-monomer) is counted the same as a

type B. The composition of the intermolecular neighbors of a particular monomer is thus defined $\phi_A = S_A/(S_A+S_B)$ and $\phi_B = 1-\phi_A$. The choice of this function and cutoff ratio was taken from similar measurement previously obtained by Medapuram et al. [14]. A probability distribution of values of ϕ_A is then constructed for test monomers of types A, B, and C in order to characterize the distribution of local environments of different monomer types. Six separate simulations were run at various values of $\chi_e N$ for chains of length $N = 16$ and $N = 32$.

The composition distributions for chains of 32 beads are shown in Figure 3.1. Values of $\chi_e N$ shown in the plots were computed using the relationship between $\chi_e(\alpha)$ and α obtained for this model in previous work [14]. As shown previously, the environment of A and B monomers becomes very different in the disordered phase near the ODT, as monomers of the same type cluster into domains to reduce AB contacts. The results also show, however, that the distribution of composition for the environment of a C end group monomer is remains quite similar to that of a randomly chosen B monomer at values of $\chi_e N$ up to the ODT, which occurs in this system at $\chi_e N = 19.57$. Slightly larger differences between the environments of B and C monomers found deeper in the ordered phase, as shown by the last plot at $\chi_e N = 34.26$, but the difference remains rather small over the range of parameters studied here.

3.2 Composition Profile in the Lamellar Phase

In the ordered phase, the average volume fraction of different monomer types become spatially inhomogeneous. This section presents measurements of the volume fractions of A, B, and C monomers as functions of one-dimensional positions within one period of lamellar phase. The main goal is to measure the extent to which the spatial

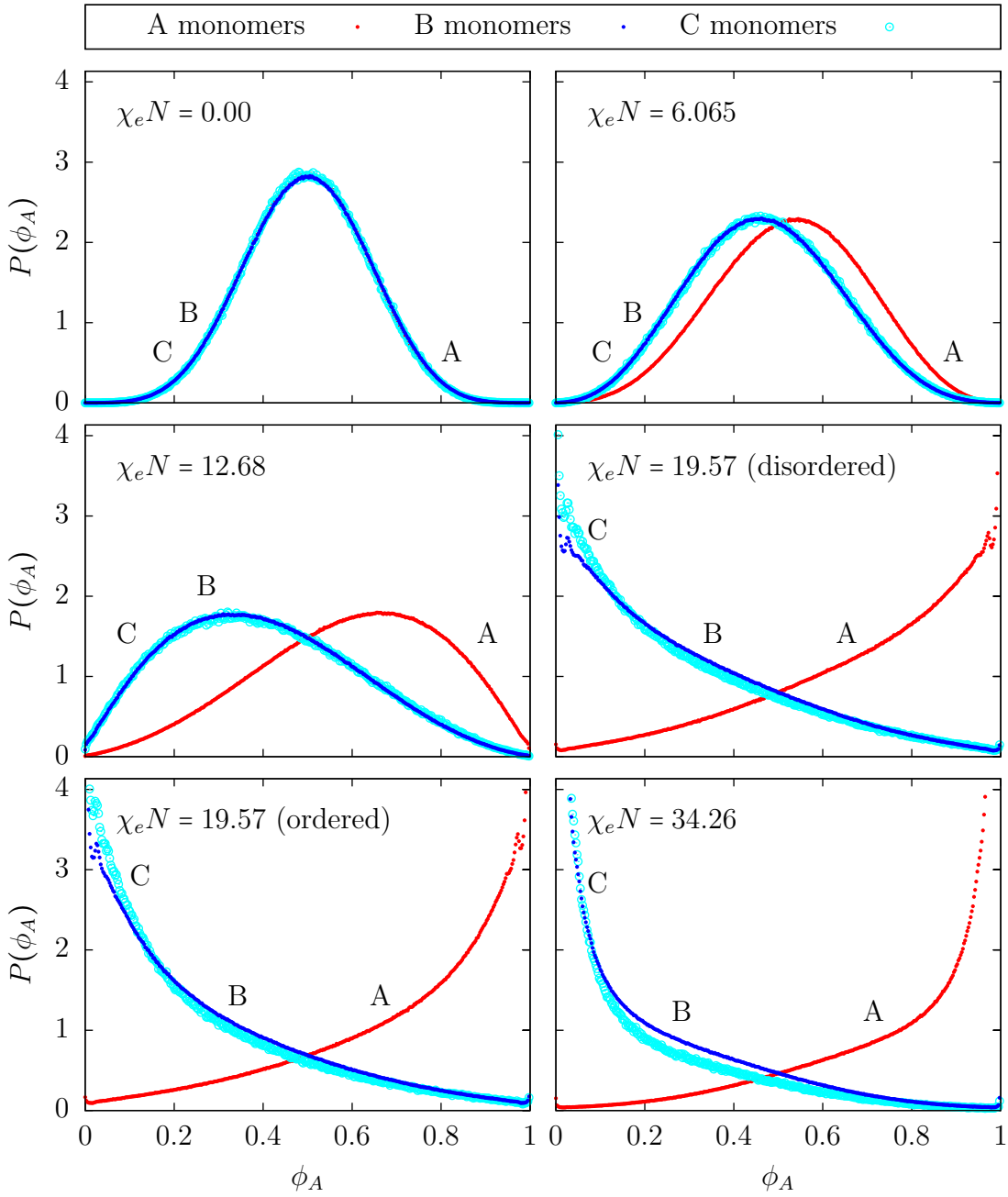

Figure 3.1: Probability distributions for the fraction ϕ_A of intermolecular neighbors around monomers of types A, B, and C for model S1-N32

distribution of C monomers differs from that of B monomers. Specifically, we would like to quantify the extent to which C monomers are concentrated near the B-rich domain and away from the interfaces between A-rich and B-rich domains. Results are also compared here to SCFT predictions for the composition profiles.

Results of the measurement of local environments presented in the previous section showed relatively little difference between local environment of B and C monomers. We would expect this to be true in the ordered phase if B and C monomers have a similar average spatial distribution. The measurement presented here allow us to determine if this is the case.

Initial measurements of the composition profile were gathered using a simple algorithm which computes the fraction of beads of each type within narrow slices constructed parallel to the layers of an ordered lamellar phase, in which each slice corresponds to a narrow range of values of a coordinate x measured orthogonal to the layers. Simulations were carried out in a cubic unit cell by using an external field that distinguishes A and B monomers to "seed" a lamellar phase with 3 layers oriented perpendicular to one of the main cubic axes.

We define an origin for the x coordinate such that $x = 0$ lies in the middle of the B/C domain. In order to locate this plane, and to order correct for any drift in the position of the layers relative to the simulation cell over the course of a long simulation, we compute the value of the third Fourier amplitude (i.e., for a system with three layers) of a field

$$\psi(\mathbf{x}) = c_A(\mathbf{x}) - c_B(\mathbf{x}) - c_C(\mathbf{x}) \tag{3.2}$$

in a simulation containing K layers, and adjust the origin of the coordinate system such that amplitude associated with this mode within a complex Fourier expansion

is a real number. (This is equivalent to using an expansion in both sines and cosines, and adjusting the origin such that the coefficient of sine component is equal to zero for this mode.) This calculation is done at each time step at which we evaluate the volume fraction, in order to determine an instantaneous position of the origin of x. Values of x relative to this origin are then collected into a separate histogram for each type of atom to produce the final composition profiles.

When the composition profile is computed as described above, the results are "smeared" somewhat by the effect of "capillary wave" undulations of interfaces between A- and B-rich domains. The effects of these undulations are not taken into account in SCFT, and are one reason for discrepancies between simulation results and SCFT predictions for composition profiles. To mitigate the effect of capillary waves, we developed an algorithm in which the simulation volume was sliced into a square grid of columns, in which each column is oriented perpendicular to the layers, as shown in Figure 3.2. An analysis similar to that originally applied to the entire system is then applied to each column, while allowing the origin of the x coordinate to be different in different columns. The overall composition profile is then obtained by combining results obtained in different columns, using an x coordinate for beads in each column that is defined relative to the position of the origin computed for that column. The use of a different coordinate system in each column allows us to correct for the effects of simple undulation modes in which all three layers bend coherently (i.e., with the same normal displacement in each layer), but does not correct for the effects of modes in which different interfaces fluctuate incoherently.

The number of cuts of the simulation box was tuned empirically to produce a balance between two conflicting considerations. Increasing the number of cuts will give a finer resolution on where the interface exists at different points in the Y,Z plane. However, too many cuts will reduce the number of monomers in a given slice,

which also tends to result in a smearing of the interface. A 15×15 grid was chosen for our final results.

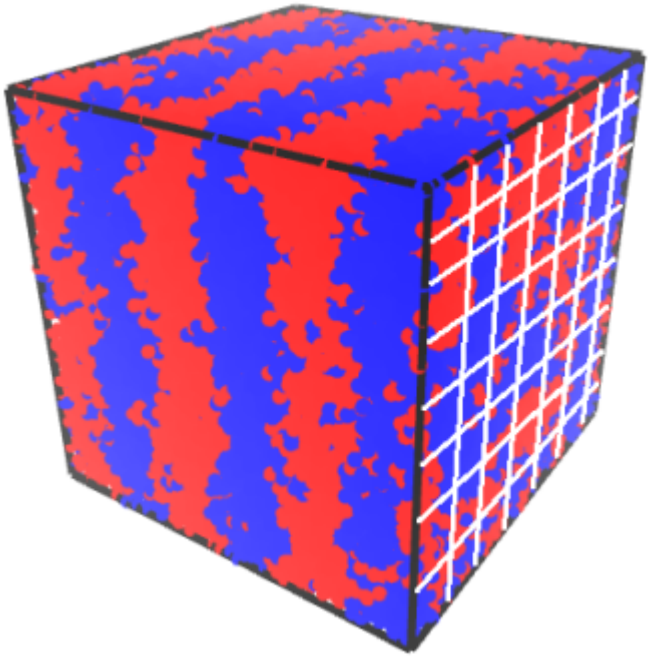

Figure 3.2: Illustration of capillary waves and simulation box cuts to minimize their effect

Composition profiles obtained with both of the algorithms described above are presented in Fig. 3.3, along with SCFT predictions. SCFT predictions were computed using the PSCF package [Source code available at github.com/dmorse/pscf.git] Results shown for two different values of $\chi_e N$ (or α), corresponding to the value at the ODT and a value well above the ODT. Simulation results obtained using a 15×15 grid of columns (dotted lines) are only slightly less smeared than those obtained using the simple algorithm (solid lines). Simulation results analyzed using either method exhibit somewhat wider interfaces than those predicted by SCFT (dot-dashed lines).

Figure 3.4 shows a comparison of results for the B monomer volume fraction $\phi_B(x)$ to $15 \times \phi_C(x)$, for chains of length $N = 32$ with 15 B monomers and 1 C monomer. Both sets of results were obtained using the simple algorithm. The results obtained in the ordered phase at the ODT show that the distribution of C monomers

is only slightly more concentrated near the middle of the B rich domain than the distribution of B monomers. Results obtained well-above the ODT show a somewhat greater tendency for C to concentrate in the middle of the B-rich domain, away from the A-rich domain. The fact that the spatial distribution of C monomers is so similar to that of B monomers at the ODT suggests that C and B monomers should be almost equally likely to come into contact with A monomers, consistent with the results of the previous section showing a very similar distribution of compositions for local environments. This conclusion also indicates that, despite the fact that the lamellar phase near the ODT has rather strongly segregated A and B domains, the value of $\chi_e N$ at the ODT of this model system is not large enough to cause significant stretching of the A and B blocks away from the interface.

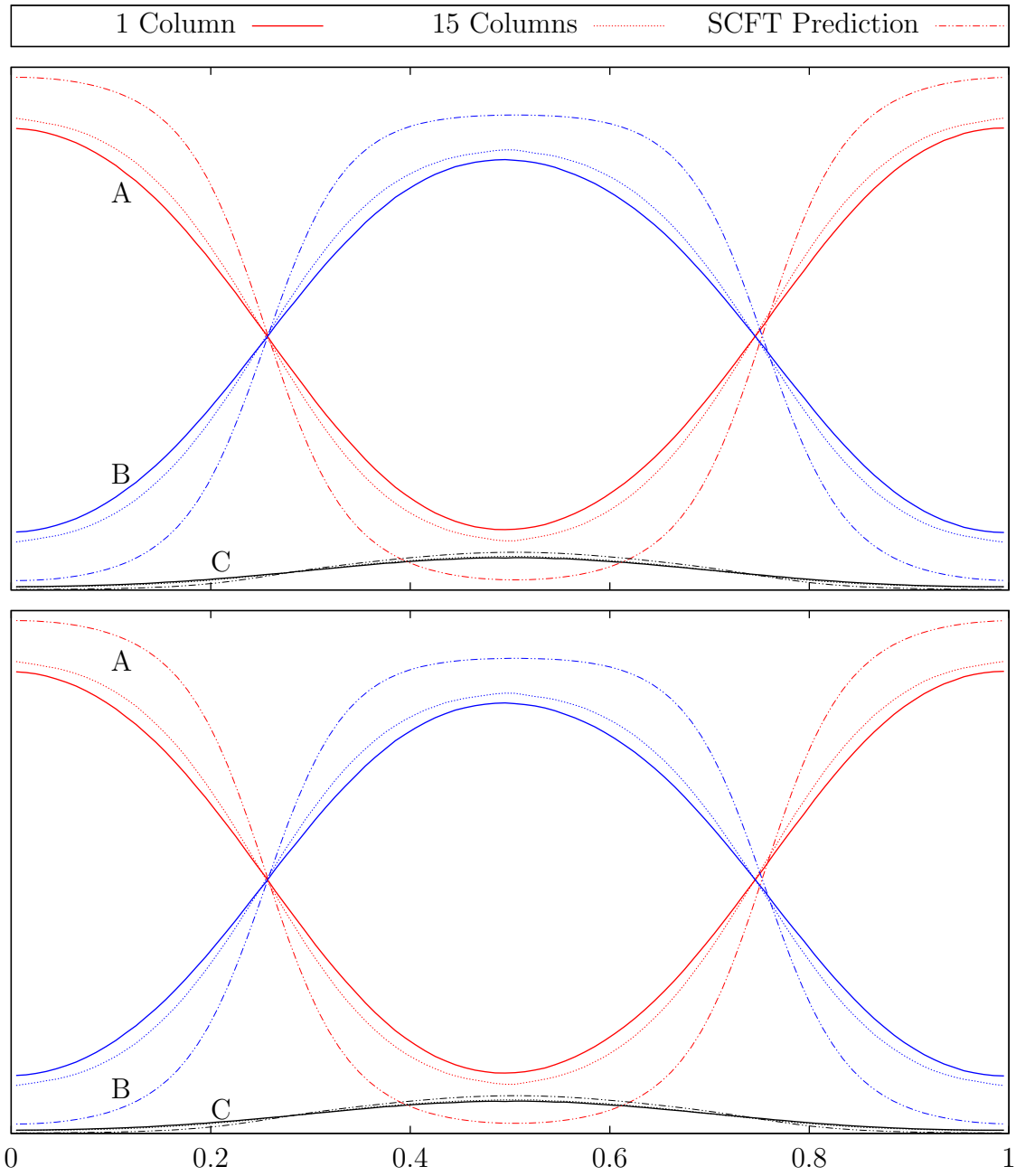

Figure 3.3: Simulation results and SCFT predictions for the average volume fraction of A, B and C monomers in the lamellar phase as a function of coordinate x measured normal to the layers, for chains with N = 32 beads per chain. The top plot shows results at $\chi_e N$ = 19.57 (α = 2.22), which is the value at the ODT, while the bottom plot shows results at higher value of $\chi_e N$ = 34.26 (α = 34.26), deep in the ordered phase. Results obtained with the simple algorithm are shown as solid lines, results with obtained using a 15×15 grid of columns are shown as dotted lines, and SCFT predictions are shown as dot-dashed lines.

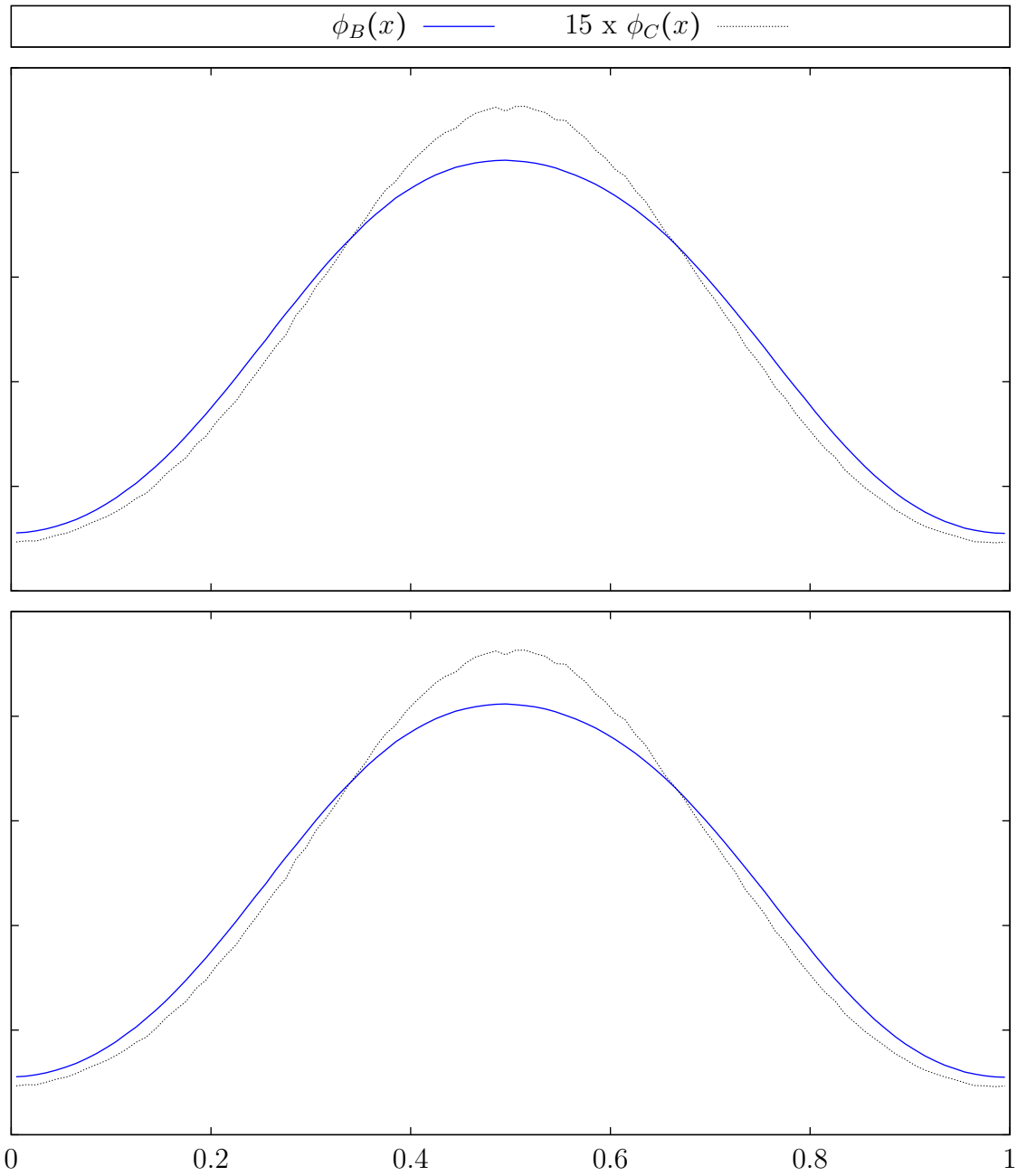

Figure 3.4: Comparison of the volume fraction $\phi_B(x)$ of B monomers to 15 times the volume fraction $\phi_C(x)$, for chains with 15 B monomers and 1 C monomer per chain, at the ODT values of $\chi_e N = 19.57$ (top) and at $\chi_e N = 34.26$ (bottom)

Chapter 4

Shift in the ODT

This chapter presents three different complementary ways of estimating how much the location of the order-disorder transition of an AB diblock copolymer is shifted if the end-monomer of the B block is replaced by a monomer of distinct type C that has a stronger repulsive interaction with A monomers. All studies reported here were carried out a melt of chains of $N = 16$ monomers, using the model described in chapter 2. It is known from previous work [14] that the AB diblock undergoes a phase transition when the parameter $\alpha = (\epsilon_{AB} - \epsilon_{AA})$ reaches a critical value of $\alpha = \alpha_{AB} = 4.92$, in energy units in which $k_B T = 1$. We study how much the critical value α_{ODT} of α_{AB} is decreased when we replace the last B monomer by a C monomer for which $\alpha_{AC} = 1.4\alpha$, as described in chapter 2. In section 3.1, we obtain upper and lower bounds on α_{ODT} by studying the spontaneous melting of systems that are prepared in a lamellar phase and spontaneous ordering of systems that are initially disordered. In section 3.2, we obtain an estimate of the ODT by extrapolating from the reference system with $\alpha_{AC} = \alpha_{BC}$ using an analysis analogous to the Clapeyron equation for the dependence of a phase boundary on system parameters. In section 3.3, we obtain a more precise estimate of α_{ODT} by using well-tempered metadynamics.

4.1 Spontaneous Phase Transitions and Hysteresis

The simplest way to estimate the location of the equilibrium ODT is by identifying the ranges of parameter values over which simulation model will exhibit spontaneous phase transformations between ordered and disordered phases. This was the method we attempted first.

To study spontaneous phase transformations, we perform two sets of simulations from different initial configurations. One set of simulations is performed starting from a disordered configuration. The other is performed by starting from an ordered lamellar configuration. Independent simulations with both initial conditions are performed at a sequence of evenly spaced values of the control parameter $\alpha = \alpha_{AB}$, over a range that is designed to include our initial guess of the value α_{ODT}, with $\alpha_{AC} = 1.4\alpha_{AB}$ in all simulations. There is a range of values of α near α_{ODT} within which either an ordered or disordered phase can exist for hundreds of millions of MD time steps without a phase transition occurring. An upper bound on α_{ODT} may be obtained by identifying the apparent melting point, which is the lowest value of α in the sequence for which an initially disordered configuration is observed to spontaneously order into a lamellar phase. A lower bound on α_{ODT} obtained by identifying the apparent freezing point, which is the highest value of α at which we observe spontaneous melting of an initially ordered system. Values of these apparent freezing and melting points depend somewhat upon the length of the simulation and the spacing between neighboring value of α, but tend to become closer together for longer simulations.

Our choice of the range of values of α over which to conduct such a study was refined by an iterative procedure. The basic procedure is, for each iteration, to run a sequence of simulations over some range of values of α, identify the freezing and melting points for this sequence, and use freezing and melting points as the minimum

and maximum values of α for the next iteration, while taking the number of MD steps in each iteration to be greater than that used in the previous iteration. Following this procedure, we first ran a set of simulations of 40 million MD steps over a range of values $\alpha \in [3.6, 5.6]$, then a set of simulations of 60 million steps over a range $[4.4, 5.0]$, and a final set of simulations of 100 million MD steps over a range $[4.53, 4.8]$. Details of this process are shown in Table 4.1.

Iteration	Duration [Timesteps]	Lower Bound	Upper Bound	Freeze Point	Melt Point
0	40 million	3.6	5.6	5.0	4.4
1	60 million	4.4	5.0	4.8	4.53
2	100 million	4.53	4.8	4.65	4.57

Table 4.1: Details of MD simulations run to narrow down a range for α_c

Identification of the final state of each of these simulations as disordered or ordered lamellar state was performed by a combination of examination of the structure factor $S(q)$ and (when necessary to resolve ambiguities) visualization of the final configuration. The appearance of coherent layers is readily apparent in a visualization of the final configuration. Measurements of $S(q)$ in each final state were obtained by averaging results obtained in an additional simulation of 10 million steps that performed after the longer annealing simulations discussed above. Figure 4.1 show examples of the results for $S(q)$ obtained from the final round of simulations that were performed using an ordered lamellar initial configuration. The structure factor $S(q)$ is measured only at discrete values of the wavenumber q that correspond to a set of symmetry related wavevectors that are commensurate with the periodic simulation cell. The value of $S(q)$ at each allowed value of q is shown as a vertical line in each plot. The existence of an ordered phase can be identified by the existence of a single value of q at which $S(q)$ is much larger than at any other value, corresponding to a Bragg peak in results of a scattering experiment.

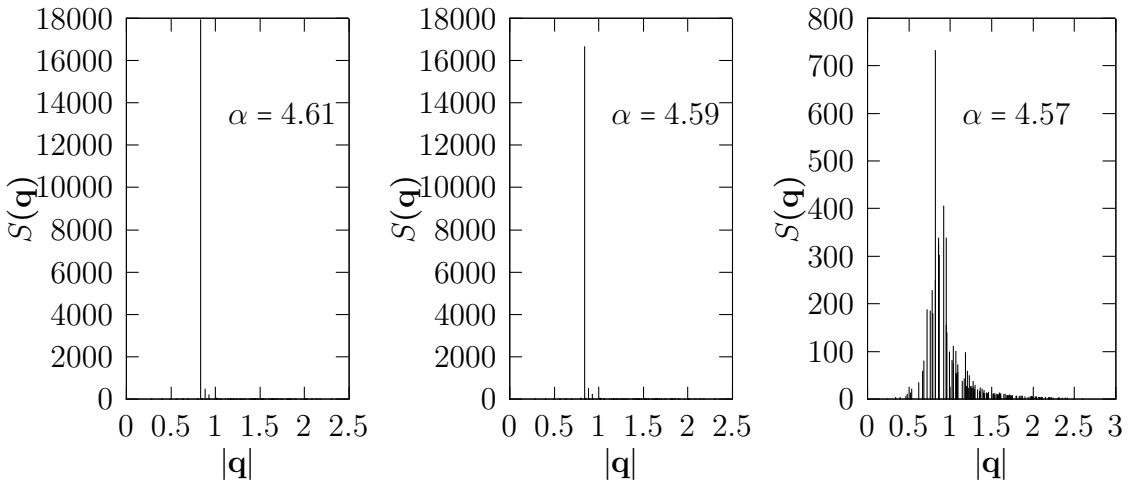

Figure 4.1: Plots of scattering structure factor $S(\mathbf{q})$ vs $|\mathbf{q}|$ of simulations that were performed with an ordered lamellar initial state. Systems with α = 4.61 and 4.59 remained in the lamellar phase, as indicated by the existence of a Bragg peak, while the system with α = 4.57 melted, as indicated by the appearance of a broader peak characteristic of a disordered block copolymer melt near the ODT. The Bragg peak in the ordered system has indices (300), corresponding to the primary peak of an ordered configuration with three layers oriented with normal vector parallel to the x axis of a periodic unit cell.

The last and longest set of these simulations of 100 MD steps yielded an apparent freezing point of α = 4.57 and a melting point of α = 4.65. These results indicate that α_{ODT} to be within the range

$$4.57 < \alpha_{\mathrm{ODT}} < 4.65 \quad . \tag{4.1}$$

This is a shift of approximately -6% from the value of α_{ODT} = 4.92 obtained by Glaser, Medapuram and coworkers for the corresponding AB diblock copolymer in the absence of an end-monomer effect. Note that the uncertainty in the value of α_{ODT} obtained by this method, while not negligible, is already significantly less than the shift in the value of α_{ODT} caused by the introduction of an end-monomer effect.

4.2 Generalized Clapeyron Equation

Another estimate of the location of the ODT was obtained by using a generalization of the Clapeyron equation to estimate the shift in $\alpha_{\rm ODT}$ arising from the replacement of the last B monomer in an AB diblock copolymer by a C monomer with different pair interactions. This provided a check on the thermodynamic consistency of the results obtained by studying spontaneous transitions.

Consider a system in which α_{AB} and α_{BC} are treated as independent parameters. The phase transition between ordered and disordered phases will define a line in a plane with coordinates α_{AB} and α_{BC}. This line will pass through the point $\alpha_{AB} = \alpha_{AC} = 4.92$ corresponding to the order-disorder transition of an AB diblock copolymer. We may estimate the shift in the value of $\alpha = \alpha_{AB}$ by determining the slope of the coexistence line in this plane, and determining where the resulting line of phase transitions intersects the line $\phi_{AC} = 1.4\alpha_{AB}$ along which our simulations were performed.

Along the order disorder transition line the Gibbs free energies of the two phases must be equal, giving

$$G_{\rm o}(\alpha_{AB}^{\rm ODT}, \alpha_{AC}^{\rm ODT}) = G_{\rm d}(\alpha_{AB}^{\rm ODT}, \alpha_{AC}^{\rm ODT}) \tag{4.2}$$

where $G_{\rm o}$ denotes the Gibbs free energy of the ordered phase and $G_{\rm d}$ denotes the free energy of the disordered phase. For an infinitesimal change in parameters such that the change of state follows the coexistence line, we require that

$$dG_{\rm o} = dG_{\rm d} \quad . \tag{4.3}$$

Expanding $dG_{\rm o}$ and $dG_{\rm d}$ to first order in the changes $d\alpha_{AB}$ and $d\alpha_{AC}$ yields the

relationship

$$\left(\frac{\partial G_o}{\partial \alpha_{AB}}\right) d\alpha_{AB} + \left(\frac{\partial G_o}{\partial \alpha_{AC}}\right) d\alpha_{AC} = \left(\frac{\partial G_d}{\partial \alpha_{AB}}\right) d\alpha_{AB} + \left(\frac{\partial G_d}{\partial \alpha_{AC}}\right) d\alpha_{AC} \tag{4.4}$$

By solving for the ratio $d\alpha_{AC}/d\alpha_{AB}$, which gives the slope of the coexistence line, we then obtain

$$\frac{\partial \alpha_{AC}}{\partial \alpha_{AB}} = -\frac{\Delta\Theta_{AB}}{\Delta\Theta_{AC}} \tag{4.5}$$

where we have defined a quantity

$$\Delta\Theta_{ij} \equiv \frac{\partial G_{\mathrm{o}}}{\partial \alpha_{ij}} - \frac{\partial G_{\mathrm{d}}}{\partial \alpha_{ij}} \tag{4.6}$$

for $ij = AC$ and $ij = BC$. This is the analog of the Clapeyron equation for the slope of a phase coexistence line of a simple substance in the temperature pressure plane.

To relate the required derivatives of G to measurable quantities, we start with the statistical mechanical relationship

$$G = -kT \ln Z \quad , \tag{4.7}$$

in which Z is the isobaric partition function,

$$Z = \int d\Gamma \exp\left(-\left[H + PV\right]/kT\right) \quad . \tag{4.8}$$

Here, $\int d\Gamma$ denotes an integral over microstates, which in NPT ensemble is an integral over particle positions and momenta and over values of the overall system volume. Differentiation of G with respect to a parameter α_{ij} yields

$$\frac{\partial G}{\partial \alpha_{ij}} = \frac{1}{Z} \int d\Gamma \frac{\partial H}{\partial \alpha_{ij}} e^{-(H+PV)/kT} = \left\langle \frac{\partial H}{\partial \alpha_{ij}} \right\rangle \tag{4.9}$$

The parameters α_{AC} and α_{AB} appear in the Hamiltonian as additive shifts in the values of the prefactors $\epsilon_{AC} = \epsilon + \alpha_{AC}$ and $\epsilon_{AB} = \epsilon + \alpha_{AB}$ of the total pair energies arising from AC and AB interactions. As a result it is straightforward to show that, in either phase,

$$\frac{\partial G}{\partial \alpha_{AB}} = \frac{\langle V_{AB} \rangle}{\epsilon_{AB}} \qquad \frac{\partial G}{\partial \alpha_{AC}} = \frac{\langle V_{AC} \rangle}{\epsilon_{AC}} \tag{4.10}$$

where $\langle V_{ij} \rangle$ denotes the average of the total pair energy arising from interactions between monomers of types i and j. It follows that

$$\Delta\Theta_{ij} = \frac{\langle V_{ij} \rangle_{\mathrm{o}}}{\epsilon_{AB}} - \frac{\langle V_{ij} \rangle_{\mathrm{d}}}{\epsilon_{AB}} \tag{4.11}$$

for $ij = AC$ and $ij = AB$, where $\langle \cdots \rangle_{\mathrm{o}}$ denotes an average taken in the ordered phase along the coexistence line and $\langle \cdots \rangle_{\mathrm{d}}$ denotes an average taken in the coexisting disordered phase under the same conditions.

Values of the quantities $\Delta\theta_{AB}$ and $\Delta\theta_{AC}$ have been measured at the state point $\epsilon_{AC} = \epsilon_{AB} = 4.92$ corresponding to the ODT of the unperturbed AB diblock copolymer system by measuring the AB and AC contributions to the pair energy in both the ordered and disordered phases and evaluating the relevant differences. Results of these simulations gave:

$$\frac{d\alpha_{AC}}{d\alpha_{AB}} = -4.8221 \pm 0.2198 \tag{4.12}$$

An approximation for α_{ODT} for a system with $\alpha_{AC} = 1.4\alpha_{AB}$ can then be determined by approximating the coexistence line a straight line in the α_{AB}-α_{AC} plane with this slope, and finding the intersection of this line with the line $\alpha_{AC} = 1.4\alpha_{AB}$. This calculation yields a predicted result

$$\alpha_{AB}\Big|_{\mathrm{ODT}} = 4.604 \pm 0.011 \quad . \tag{4.13}$$

This estimate is completely with the requirement from the previous measurement that $4.57 < \alpha_{AB} < 4.65$, and lies near the middle of this range of possible values.

4.3 Well-Tempered Metadynamics

The most accurate method that we have used to estimate the location of the order-disorder transition relies on the use of a well-tempered metadynamics, using a procedure that was developed for this purpose by Glaser and coworkers [13]. This section gives brief description of this well-tempered metadynamics algorithm. Our application of the method used software developed for the purpose by Dr. Jens Glaser, which was also used in the original study of the ODT of AB diblock copolymers [13].

Metadynamics is an adaptive biasing technique used to obtain the free energy surface of a system in particle-based simulations[19]. It simulates a system with a modified Hamiltonian given by a sum

$$H = H_0 + V(\Psi) \tag{4.14}$$

of the physical system Hamiltonian H_0 and a bias potential $V(\Psi)$ which depends on some collective variable Ψ. The bias potential $V(\Psi)$ evolves throughout the course of a simulation in such a way as to discourage the system from revisiting regions of the configuration space which it has already visited. This accelerates the rate of otherwise rare transitions between different regions of configuration space (in this case ordered and disordered configurations). The bias potential is constructed by depositing Gaussian shaped repulsive potentials centered around the points in configuration space that the system visits over the course of the simulation. The error resulting from the introduction of this bias potential is proportional to the square

root of the bias potential deposition rate [20] which is constant in standard metadynamics simulations. The deposition rate must be tuned to minimize this error while allowing the simulation to efficiently explore new regions of the configuration space. Well-tempered metadynamics improves on standard metadynamics by introducing a potential of the form

$$V(\Psi, t) = \Delta T \ln\left[1 + \frac{\omega N(\Psi, t)}{\Delta T}\right], \tag{4.15}$$

where ω has the dimension of an energy rate, ΔT is a tunable shift temperature, and $N(\Omega, t) = \int_0^t \delta_{\Omega,\Omega(t')} dt'$ is the histogram of the collective variable Ω[21]. This potential is advantageous because it has a time derivative of the form

$$\dot{V}(\Omega, t) = \omega e^{-[V(\Omega,t)/\Delta T]} \delta_{\Omega,\Omega(t)}. \tag{4.16}$$

Equation 4.16 has two important properties. The first is that it tends to zero as $1/t$ which allows the system to eventually converge. The second is that $\dot{V}(\Omega)$ is not uniform in Ω-space so that the deposition rate is inversely proportional to the time already spent in configurations with given value of Ω. At the end of the simulation, the free energy surface can be reconstructed up to a constant by taking the negative of the bias potential

$$G(\Psi) = -\frac{T + \Delta T}{T} V(\Psi) + C \tag{4.17}$$

where T denotes the temperature of the system.

A key component in the design of these types of algorithms is the choice of an optimal collective variable function. Appropriate choices for the collective variable Ψ to identify the order-disorder transition can be any differentiable function of the particle positions that yields easily distinguishable values in the ordered and disordered

states [14]. We chose a collective variable function of the form

$$\Psi \equiv \left[\Sigma_{\mathbf{q}} |\psi(\mathbf{q})|^4 f(|\mathbf{q}|)\right]^{1/4} \tag{4.18}$$

in which $\psi(\mathbf{q})$ is a Fourier amplitude of the composition field $\psi(\mathbf{r}) = c_A(\mathbf{r}) - c_B(\mathbf{r}) - c_C(\mathbf{r})$, the sum $\Sigma_{\mathbf{q}}$ is taken over allowed wavevectors $\mathbf{q}$, and $f(|\mathbf{q}|)$ is a cutoff function that suppresses contributions from wavevectors with $|\mathbf{q}| >> \mathbf{q}^*$. This choice is analogous to a collective variable function previously chosen [14] by this group after much experimentation for the purpose of identifying the ODT in pure diblock systems.

This particular implementation of the algorithm was accelerated using multiple walkers in which weakly-coupled replicas of the system were run simultaneously to construct a common bias potential calculated by summing up the Gaussian contributions from each walker. The simulation was run for 120 million timesteps using 10 Nvidia Tesla K40m GPUs. The measured free energy surface is shown in Figure 4.2.

The well-tempered metadynamics simulation was run at a value of $\alpha = 4.65$ that is slightly above the expected ODT. We define α_{ODT} to be the value of α for which the probability of being in the ordered or disordered states are equal for a system with an equilibrium distribution of values for Ψ. We solve α_{ODT} by doing a perturbation of $P(\Psi, \alpha)$ around the point $\alpha = \alpha_0 = 4.65$ and numerically solving

$$G(\Psi, \alpha) \approx G(\Psi, \alpha_0) + \frac{\partial G(\Psi, \alpha_0)}{\partial \alpha} (\alpha - \alpha_0) \tag{4.19}$$

$$\int_0^{\Psi_{\mathrm{mid}}} \exp\left[-G(\Psi, \alpha)/k_B T\right] d\Psi = \int_{\Psi_{\mathrm{mid}}}^{\infty} \exp\left[-G(\Psi, \alpha)/k_B T\right] d\Psi. \tag{4.20}$$

This method yields $\alpha_{\mathrm{ODT}} = 4.623$. This is very close to the estimate obtained from the Clapeyron approximation and well within range of upper and lower bounds obtained

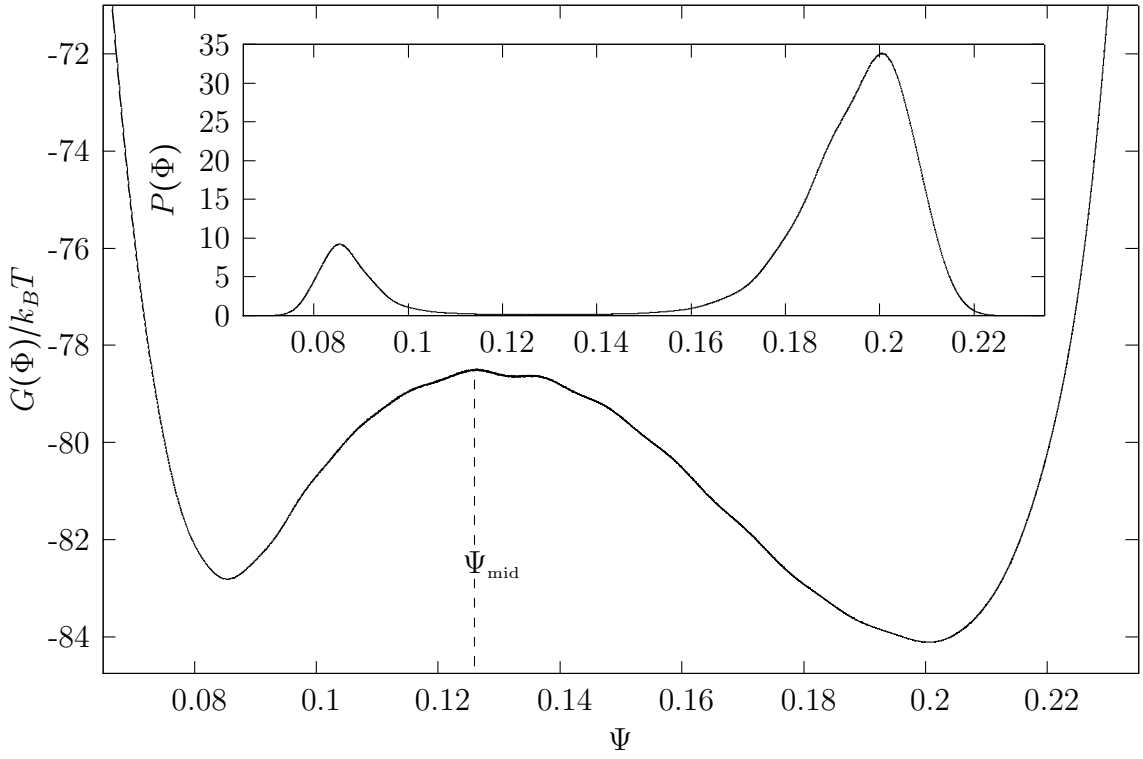

Figure 4.2: Gibbs free energy G/k_BT as a function of the order parameter Ψ measured by well-tempered metadynamics. Inset: corresponding probability distribution $P(\Psi) = \exp(-G/k_BT)/\int \exp(-G/k_BT)$.

by studying spontaneous phase transitions.

Chapter 5

Fluctuations in the Disordered Phase: Estimating $\chi_e N$

The work presented in this thesis was motivated in large part by a desire to understand the possible role of end-monomer effects in the detailed analyses of experiments on PI-PLA diblock copolymer presented by Gillard et al. [15] and, subsequently, by Beardsley and Matsen [16]. Gillard et al. noted discrepancies in the results obtained with nearly symmetric PI-PLA diblock copolymers of different molecular weights, and hypothesized that these discrepancies might be the result of an end-group effect. Beardsley and Matsen focused on improving the analysis of Gillard et al. by carefully taking into account the effects of polydispersity, which Gillard et al. neglected. Beardsley and Matsen showed that the inclusion of polydispersity within the simulations to which the experiments were compared significantly improved the level of agreement between simulations and experiment. Because Beardsley and Matsen only analyzed results obtained from a single sample, however, they did not address the questions raised by Gillard et al. about the origin of the unexpected dependence of the location of the ODT upon overall chain length.

In this section, we reconsider the hypothesis of Gillard et al. that the unexpected dependence of $(\chi_e N)_{\mathrm{ODT}}$ upon chain length in PI-PLA copolymers could be the result of an end-monomer effect. If this assumption is true, however, we must ask how

Beardsley and Matsen [16] were able to get such good agreement in their subsequent analysis of data for a single sample without accounting for an end-monomer effect. Specifically, we would like to understand if it is possible that Beardsley and Matsen could obtain agreement between their estimated values of $(\chi_e N)$ for an experiment that has a significant end-monomer effect and a simulation that does not. This might be explained if the effect of the end-monomer was implicitly taken into account by the way that they estimated the effective interaction parameter for the experimental system. Beardsley and Matsen estimated the temperature dependence of $\chi_e(T)$ for PI-PLA system by comparing the magnitude of the peak $S(q^*)$ of the structure factor obtained from scattering from the disordered phase of the PI-PLA diblock copolymer melt to simulation results for $S(q^*)$ for a system with appropriate values of $\overline{N}$ and of the polydispersity index. If the end-monomer of the lactic acid block of the PI-PLA copolymers repels PI monomers more strongly than other monomers in the block, this would tend to increase the tendency toward microphase segregation. Because this would increase the magnitude of fluctuations in the disordered phase from which $\chi_e(T)$ is estimated, this effect would yield a larger estimate of $\chi_e(T)$ at any temperature T than would be obtained in a hypothetical PI-PLA system with no end effect. The same physical effect would, however, also tend to favor formation of an ordered phase, and thus increase the value of the order-disorder temperature $T_{\rm ODT}$. Because $\chi_e(T)$ is a decreasing function of T, the resulting shift in $T_{\rm ODT}$ would by itself tend to decrease our estimate of $(\chi_e N)_{\rm ODT} = \chi_e(T_{\rm ODT})N$. We ask here whether it is possible that, when one analyzes data from a single sample, the increase in the estimate of $\chi_e(T)$ arising from an end-group effect could nearly compensate the corresponding increase in T_{ODT}, yielding an estimated value of $(\chi_e N)_{ODT}$ very similar to what one would get in the absence of an end-group effect.

We test this hypothesis by analyzing the results of simulation data for our model

of a polymer with an repulsive end-monomer in a manner closely analogous to the method used by both Gillard et al. and Beardsley and Matsen to analyze data from experiments on PI-PLA diblock copolymers. To do so, we measure the the dependence of the structure factor in the disordered phase upon α, and compare this to ROL theory predictions for a system with no end-group effect to obtain an estimate of how χ_e depends on α_{AB}. We then use the resulting calibration of $\chi_e(\alpha)$ and knowledge of the value of α_{ODT} to obtain an estimate of $(\chi_e N)_{\mathrm{ODT}}$ for a system with a measurable end-group effect. We stress that the simulations were run in the presence of an end-monomer effect, but the calibration of $\chi_e(\alpha)$ was carried out as if the effect did not exist.

Seven NPT simulations were run using the same configuration parameters outlined in section 2.2 at evenly spaced values of α_{AB} in the range $1.0 \leq \alpha_{AB} \leq 4.0$. The scattering structure factor $S(q)$ was measured at various wavevectors $\mathbf{q}$ that were commensurate with the simulation unit cell. An estimation for $\chi_e(\alpha)$ was obtained by following the same procedure outlined in Ref [22] and summarized below.

For each simulation, the continuous function $S(q)$ was interpolated by fitting the discrete data to an empirical model of the form

$$cNS^{-1}(q) \approx F(qR_{g0}) + a + bq^2 + cq^4 \tag{5.1}$$

where $F(qR_{g0})$ is part of the functional form for $S(q)$ predicted by the Random Phase Approximation [4]. The constants a, b, and c have no physical significance. The fit was restricted to points in the vicinity of the peak by only including data within the range $1.0 \leq qR_{g0} \leq 3.0$. Figure 5.1 shows an example of the behavior of $S(q)$ at several different values of α. The fit lines were used to determine the magnitude of the peak wavevectors q^* and the values of the inverse structure factor at the peak $S^{-1}(q^*)$. We

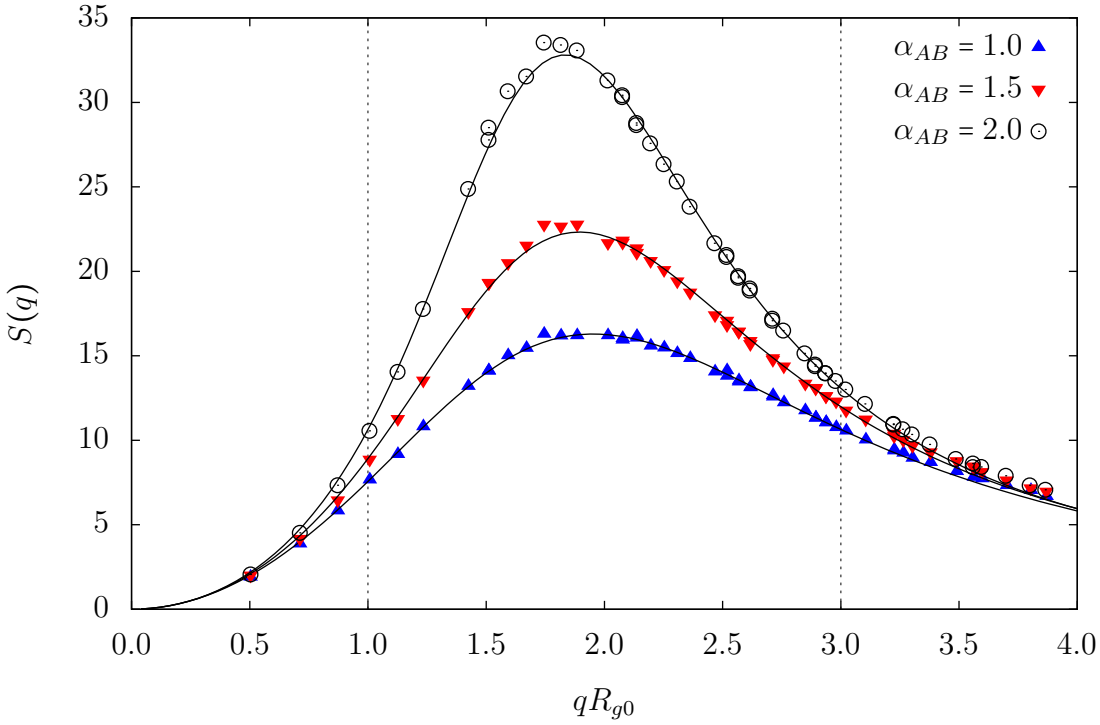

Figure 5.1: Fit of data for $S(q)$ to Equation 5.1. Only data between the dashed lines was included in the fit.

then used ROL theory predictions for $S^{-1}(q^*)$ vs. χ_e to obtain discrete pairs of points for α vs χ_e. Those points were then fit to the functional form

$$\chi_e(\alpha) = \frac{z\alpha + a_2\alpha^2}{1 + d_1\alpha} \quad , \tag{5.2}$$

while treating z, d_1 and a_2 as fitting parameters. Data with values of $cNS^{-1}(q^*) < 0.70$ was excluded from the fit to avoid possible corruption by finite size effects, as also done in Ref. [22]. Our estimate of $\chi_e N$ was then obtained by evaluating the resulting approximation for $\chi_e(\alpha)$ at the value of $\alpha_{\mathrm{ODT}} = 4.62$ obtained for this system from well-tempered metadynamics.

In order to determine the impact that the end-monomer effect has on our estimate $(\chi_e N)_{\mathrm{ODT}}$, the procedure described above was also applied to a standard symmetric

AB diblock copolymer with N = 16 beads, without a distinct end-monomer.

Figure 5.2 shows results for the normalized inverse peak scattering intensity $cNS^{-1}(q^*)/2$ vs $\chi_e(\alpha)N$ for both systems, plotted using approximations for $\chi_e(\alpha)$ for each system in which the parameters in Equation 5.2 have been chosen to fit the data to the ROL theory for A/B diblock copolymer, plotted alongside the relevant ROL theory prediction. The parameters values obtained from these fits of $\chi_e(\alpha)$ to Equation 5.2 are presented in Table 5.1. This table also contains the estimates of $(\chi_e N)_{\mathrm{ODT}}$ that are obtained by evaluating the resulting approximations for $\chi_e(\alpha)$ at the measured value of α_{ODT} for each system. The resulting estimates of $(\chi_e N)_{\mathrm{ODT}}$ for the systems with and without a distinct end-monomer differ by only 1.2% ($\chi_e N$ = 24.03 vs. 24.32), with a slightly greater value for the system with an end-effect, while the values of α_{ODT} for these two systems differ by approximately 6% (α_{ODT} = 4.92 vs. 4.62), with a greater value for the system with no end effect.

These results indicate that effects of an end-monomer upon composition fluctuations in the disordered phase and upon the ODT are sufficiently similar to the effect of a change in the value of χ_e for a diblock copolymer that, to first approximation, both effects can be absorbed into a shift in the calibration of χ_e. The implication is that it appears that it would be very difficult to discern whether or not a system has a significant end effect by applying this sort of analysis to a single sample. The presence or absence of end effects would, however, become more apparent in a comparison of chains of with the same chemistry and composition but different overall molecular weight.

The analysis used here to estimate the $\chi_e(\alpha)$ for an AB diblock copolymer is slightly different from that used previously by Glaser, Medapuram, et al. [13, 14], and yields a slightly different result. In previous work, these authors estimated $\chi_e(\alpha)$ for model S1 by simultaneously fitting results obtained from chains of length N =

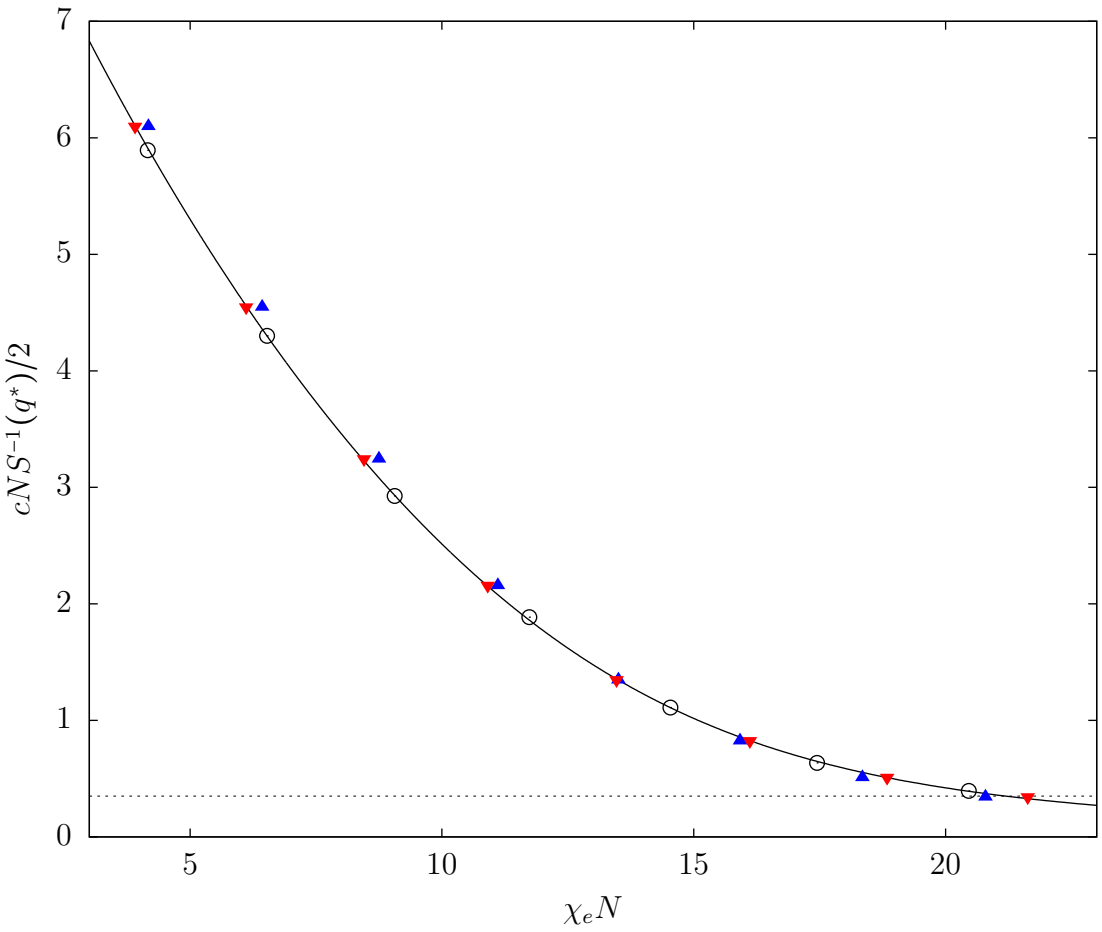

Figure 5.2: Fit of simulation results for $cNS^{-1}(q^*)/2$ vs $\chi_e N$ to ROL theory predictions. All simulation results are for copolymer melts with chains of N = 16 beads, with $\overline{N}$ = 480. Solid curve is the ROL prediction for this value of $\overline{N}$. Open circles show simulation results for ABC copolymers with 8 A beads, 7 B beads and a single C end monomer, plotted using a function $\chi_e(\alpha)$ of the form given in Equation 5.2 with parameters chosen to to fit this data to the ROL prediction. Inverted red triangles represent data from symmetric AB copolymers, fit to the ROL prediction ins the same manner. Blue triangles represent the same set of data from symmetric AB diblock copolymers of length N = 16 plotted using the relationship for $\chi_e(\alpha)$ obtained in previous work [13, 14] from a more constrained simultaneous fit of results from chains of varying length. Only points above the dashed line, for which $cNS^{-1}(q^*)/2 > 0.35$, were included in the fits of $\chi_e(\alpha)$ to Equation 5.2

$12, 16, 32, 64$, and 128 to the ROL theory, whereas only data from chains of length N = 16 was used in the analysis presented here. Their calibration of $\chi_e(\alpha)$ also

Simulation Model	z	a_2	d_1	α_{ODT}	$(\chi_e N)_{\mathrm{ODT}}$
N=16, no end-effect	0.220	0.054	0.119	4.92	24.03
N=16, with end-effect	0.232	0.054	0.101	4.62	24.32

Table 5.1: Values obtained for parameters in Equation 5.2 for $\chi_e(\alpha)$, values of α_{ODT}, and resulting estimates of $(\chi_e N)_{\mathrm{ODT}}$ for copolymer melts with and without a distinct C end monomer.

differed from that presented here in that they used a fixed value for z that had been independently determined from an analysis of the structure of a homopolymer reference state, whereas z was treated as a freely adjustable fitting parameter in the analysis presented here. The analysis given here was designed to imitate the analysis presented by Beardsley and Matsen (applied here to a monodisperse system), in that the estimate of χ_e was determined entirely from a fit of scattering data from a single sample. A simultaneous fit to data from multiple chain lengths could not have been applied to the system with an end-monomer because the end-monomer effect is, of course, chain-length dependent. Figure 5.2 displays the results obtained using the multi-chain calibration alongside the results of our calibration. Because the earlier analysis was based on a simultaneous fit to data from several chain lengths using a functional form with one fewer adjustable parameter than that used here, it naturally does not fit the data for chains of length N = 16 quite as well as our fit to only this data. It is worth noting, however, that the calibration given by these authors yields a value of $(\chi_e N)_{ODT}$ = 22.76 for AB diblock copolymers of length N = 16 that is about 6 % lower than the estimate of $(\chi_e N)_{\mathrm{ODT}}$ = 24.03 obtained here by using a different fitting procedure to estimate $\chi_e(\alpha)$ for the same system. This shows that values of χ_e that are obtained by fitting scattering results to the ROL predictions can depend somewhat more on details of the fitting procedure than had previously been appreciated. This discrepancy does not, however, effect our conclusions regarding the relationship between the system with and without an end-group effect, because

our comparison of those two systems was performed by applying the same fitting procedure to both systems.

Chapter 6

Discussion and Conclusions

We have analyzed and presented coarse-grained simulation measurements of end-monomer effects in diblock copolymer melts. Our first focus was characterizing the local environment around the end-monomer and comparing it to the other monomers on the chain. Local monomer composition distributions and composition profiles were also measured to characterize the end-monomers position within the bulk relative to the other monomers. Our results indicated that the local environment around the end-monomer was not significantly different than the other monomers.

Our second focus was to measure the shift in the position of the ODT due to a repulsive end-monomer effect. The location of the ODT was first determined within a range of 1.7% by spontaneous ordering and melting. The position of the ODT was then approximated by deriving a Clapyron-style relationship to characterize the shape of the coexistance curve between the ordered and disordered phases. This approximation agreed with the range measured by spontaneous ordering. The precise position of the ODT was then determined by well-tempered metadynamics simulations. Finally we measured the repulsive end-monomer's effect on the position of $(\chi_e N)_{\text{ODT}}$ by fitting scattering measurements in the disordered phase to ROL theory predictions. Our results indicate that the end-monomer's effect on measurements in the disordered phase are indistinguishable from its effect on the ODT. The system

has nearly the same value for $(\chi_e N)_{\mathrm{ODT}}$ with and without the end-monomer effect. Thus the end-monomer will have an N-dependant effect on the ODT, but it will be very difficult to detect if the calibration for χ_e is restricted to measurements of a single chain length.

Bibliography

[1] Michael Rubinstein and Ralph Colby. In: *Polymer Physics*. 2003. Chap. 4.

[2] Paul J. Flory. In: *Principals of Polymer Chemmistry*. 1953. Chap. 12.

[3] M. W. Matsen. "The standard Gaussian model for block copolymer melts". In: *J. Phys.: Condensed Matter* (2002).

[4] Ludwik Leibler. "Theory of Microphase Separation in Block Copolymers". In: *Macromolecules* (1980).

[5] S. A. Brazovskii. "Phase transition of an isotropic system to a nonuniform state". In: *Soviet Physics JETP* (1975).

[6] G. H. Fredrickson and Eugene Helfand. "Fluctuation effects in the theory of microphase separation in block copolymers". In: *The Journal of Chemical Physics* (1987).

[7] A. V. Dobrynin and I. Ya. Erukhimovich. "Fluctuation effects in the theory of weak supercrystallization in block copolymer systems of complicated chemical structure". In: *Journal de Physique II* (1991).

[8] Jean-Louis Barrat and Glenn H. Fredrickson. "Collective and single-chain correlations near the block copolymer order-disorder transition". In: *The Journal of Chemical Physics* (1991).

[9] L. Kielhorn and M. Muthukumar. "Fluctuation theory of diblock copolymer/homopolymer blends and its effects on the Lifshitz point". In: *The Journal of Chemical Physics* (1997).

[10] Alexander Kudlay and Semjon Stepanow. "Short-range fluctuations in the Hartree theory of diblock copolymer melts". In: *The Journal of Chemical Physics* (2003).

[11] Monica Olvera de la Cruz. "Transitions to periodic structures in block copolymer melts". In: *Physical Review Letters* (1991).

[12] J. Qin P. Grzywacz and D. Morse. "Renormalization of the one-loop theory of fluctuations in polymer blends and diblock copolymer melts". In: *Physical Review Letters* (2007).

[13] J. Glaser et al. "Universality of Block Copolymer Melts". In: *Physical Review Letters* (2014).

[14] Pavani Medapuram Jens Glaser and David C. Morse. "Universal Phenomenology of Symmetric Diblock Copolymers near the Order-Disorder Transition". In: *Macromolecules* (2015).

[15] D. Morse T. Gillard P. Medapuram and F. Bates. "Fluctuations, Phase Transitions, and Latent Heat in Short Diblock Copolymers: Comparison of Experiment, Simulation, and Theory". In: *Macromolecules* (2015).

[16] T. M. Beardsley and M. W. Matsen. "Universality between Experiment and Simulation of a Diblock Copolymer Melt". In: *Physical Review Letters* (2016).

[17] R. D. Groot and T.J. Madden. "Dynamic simulation of diblock copolymer microphase separation". In: *The Journal of Chemical Physics* (1998).

[18] et al J. Glaser J. Quin. "Test of scaling hypothesis for the structure factor of disordered diblock copolymer melts". In: *Soft Matter* (2012).

[19] A. Laio and M. Parrinello. "Escaping free-energy minima". In: *Proc. Natl. Acad. of Sci. USA* (2002).

[20] M. Parrinello G. Bussi A. Laio. "Equilibrium free energies from non-equilibrium metadynamics". In: *Physical Review Letters* (2006).

[21] G. Bussi A. Barducci and M. Parrinello. "Well-tempered metadynamics: A smoothly converging and tunable free-energy method". In: *Physical Review Letters* (2008).

[22] et al J. Glaser J. Quin. "Collective and Single-Chain Correlations in Disordered Melts of Symmetric Diblock Copolymers: Quantitative Comparison of Simulations and Theory". In: *Macromolecules* (2014).